

Influence of Gas Atmosphere Dew Point on the Galvannealing of CMnSi TRIP Steel

LAWRENCE CHO, MYUNG SOO KIM, YOUNG HA KIM,
and BRUNO C. DE COOMAN

The Fe-Zn reaction occurring during the galvannealing of a Si-bearing transformation-induced plasticity (TRIP) steel was investigated by field-emission electron probe microanalysis and field-emission transmission electron microscopy. The galvannealing was simulated after hot dipping in a Zn bath containing 0.13 mass pct Al at 733 K (460 °C). The galvannealing temperature was in the range of 813 K to 843 K (540 °C to 570 °C). The kinetics and mechanism of the galvannealing reaction were strongly influenced by the gas atmosphere dew point (DP). After the galvannealing of a panel annealed in a N₂ + 10 pct H₂ gas atmosphere with low DPs [213 K and 243 K (−60 °C and −30 °C)], the coating layer consisted of δ (FeZn₁₀) and η (Zn) phase crystals. The Mn-Si compound oxides formed during intercritical annealing were present mostly at the steel/coating interface after the galvannealing. Galvannealing of a panel annealed in higher DP [263 K and 273 K, and 278 K (−10 °C, 0 °C, and +5 °C)] gas atmospheres resulted in a coating layer consisting of δ and Γ (Fe₃Zn₁₀) phase crystals, and a thin layer of Γ_1 (Fe₁₁Zn₄₀) phase crystals at the steel/coating interface. The Mn-Si oxides were distributed homogeneously throughout the galvannealed (GA) coating layer. When the surface oxide layer thickness on panels annealed in a high DP gas atmosphere was reduced, the Fe content at the GA coating surface increased. Annealing in a higher DP gas atmosphere improved the coating quality of the GA panels because a thinner layer of oxides was formed. A high DP atmosphere can therefore significantly contribute to the suppression of Zn-alloy coating defects on CMnSi TRIP steel processed in hot dip galvanizing lines.

DOI: 10.1007/s11661-013-1867-8

© The Minerals, Metals & Materials Society and ASM International 2013

I. INTRODUCTION

IMPROVED safety standards and a trend toward automotive body-in-white weight containment have led to a strong interest in advanced high strength steels (AHSS) such as transformation-induced plasticity (TRIP) steel. The Zn coating of TRIP steel by means of hot dip galvanizing (HDG) and galvannealing is a key factor which determines whether TRIP steel can be used in automotive body-in-white construction, as thin TRIP steel sheets used for lighter car bodies should be resistant to perforation corrosion.

The HDG process is used to produce pure Zn (η)-coated steel by the hot dipping of recrystallization-annealed strips into an Al-containing Zn bath. The Al content of the Zn bath for galvanized sheet production is typically 0.2 mass pct Al. Production of galvannealed (GA) sheet steel consists of two processes: the galvanizing itself and the subsequent short diffusion annealing process lasting ~20 s in the range from 763 K to 823 K

(490 °C to 550 °C). The latter process step transforms the Zn layer into an Fe-Zn alloy layer by interdiffusion and reaction of Fe and Zn. This results in the formation of Fe-Zn intermetallic compounds.

The reaction between Fe in the solid state and Zn in the liquid state during the galvannealing results in the formation of the coating layer which may contain the following Fe-Zn intermetallic compounds: zeta (ζ)-FeZn₁₃, delta (δ)-FeZn₁₀, gamma₁ (Γ_1)-Fe₁₁Zn₄₀, and gamma (Γ)-Fe₃Zn₁₀ phases. The Fe content and structure of the Fe-Zn intermetallic compounds in GA coating should be properly controlled to minimize powdering. Powdering is the delamination of the coating during forming operations such as deep drawing. Coatings with a good powdering resistance have been reported to consist of a layer of Γ phase <1 μ m in thickness and the softer δ phase crystals as the main constituent with a small amount of the ζ phase crystals at the surface of the coating.^[1] The optimal coating has an average Fe content of ~10 mass pct.

The gas atmosphere in the annealing furnace of a continuous HDG line reduces the iron oxides formed during cold rolling to elemental Fe. AHSS alloyed with Mn, Si, or Al are subject to selective oxidation during annealing since the alloying elements have a high affinity for oxygen. This selective oxidation occurs at the steel surface in the low dew point (DP) gas atmosphere of HDG lines operating in standard processing conditions. The presence of film-forming surface oxides, in

LAWRENCE CHO, Graduate Student, and BRUNO C. DE COOMAN, Professor, are with the Graduate Institute of Ferrous Technology, Pohang University of Science and Technology, Pohang, 790-784, South Korea. Contact e-mail: decooman@postech.ac.kr MYUNG SOO KIM and YOUNG HA KIM, Researchers, are with the POSCO Technical Research Laboratories, Gwangyang, 545-090, South Korea.

Manuscript submitted April 10, 2013.

Article published online July 12, 2013

particular the amorphous a - x MnO·SiO₂ ($x < 0.9$) and a -SiO₂ oxides, leads to a deterioration of the wettability of the intercritically annealed strip by the molten Zn during the galvanizing process.^[2-4] These oxides are also believed to act as barriers to the interdiffusion of Fe and Zn during the galvannealing process.^[1,5-7] In this case, a higher galvannealing temperature or a longer annealing time is required to accelerate the Fe-Zn reaction kinetics. These corrective interventions are, however, often not compatible with the process window available for galvannealing in industrial continuous galvanizing lines.

The control of the DP was suggested as a promising method to improve the quality of Zn and Zn-alloy coatings. Annealing of the strip in a high DP atmosphere has been shown to result in internal oxidation rather than external oxidation.^[8-10] Although the effect of the DP on the selective oxidation has been clearly observed,^[8-14] the influence of the DP on the distribution of the oxides and the formation of Fe-Zn intermetallic phases during galvannealing has not yet been documented.

The present study focuses on the influence of the external and internal oxides on the formation of the Fe-Zn intermetallic phase crystals during the galvannealing of CMnSi TRIP steel in a HDG simulator. The oxides and the Fe-Zn intermetallic phase crystals formed during the galvannealing of the steel annealed in different DP conditions were analyzed by means of high resolution methods, field-emission electron probe microanalysis (FE-EPMA), and field-emission transmission electron microscopy (FE-TEM) of cross-sectional samples prepared by the focused ion beam (FIB) technique. The observations make it possible to propose a conceptual model for the Fe-Zn reaction in the presence of Mn-Si compound oxides formed at the steel surface during intercritical annealing (IA) in low DP conditions and in the subsurface during IA in high DP conditions.

II. EXPERIMENTAL

Industrially cold-rolled full hard CMnSi TRIP steel sheets containing 2.2 mass pct Mn and 1.4 mass pct Si were used for galvannealing simulations. The Mn/Si mass pct ratio in a TRIP steel composition is critical for the wettability of steel strip by the molten Zn. This is because different types of oxides are formed on steels with the different Mn/Si ratios during IA. When the Mn/Si mass pct ratio is high (*e.g.*, Mn/Si atomic ratio > 2), more particle-type crystalline c - x MnO·SiO₂ ($x > 1$) oxides are formed on the surface than film-type amorphous a -SiO₂ or a - x MnO·SiO₂ ($x < 1$) oxides. In general, oxides with a particle-type morphology are known to be less harmful to the wettability than film-type oxides. The Mn/Si mass pct ratio of the CMnSi TRIP steel was 1.57 and bare spots were not present in the Zn coating surface after the galvanizing simulation.^[15] The cold-rolled TRIP steel had a thickness of 1.2 mm and panels with dimensions of 220 × 120 mm were cut from the sheet. The panels were annealed and

GA in an IWATANI SURTEC HDG simulator (IWATANI Inc., Germany). This HDG simulator consists of a hot dipping simulation unit, a gas mixing station, a hybrid humidification system, and a control system. In the heating section of the main unit, an infrared furnace was used for the continuous annealing simulation and an induction furnace was used for the galvannealing. The process gasses, N₂, H₂, and He, were mixed in the gas mixing station and the gas mixture was humidified in a hybrid humidification system. The control system allowed for the precise control of the composition and the DP of the gas atmosphere.

The galvannealing was simulated on panels intercritically annealed in a N₂ + 10 pct H₂ gas atmosphere with DPs of 213 K, 243 K, 263 K, 273 K, and 278 K (−60 °C, −30 °C, −10 °C, 0 °C, and +5 °C). The gas atmospheres with DPs of 213 K and 243 K (−60 °C and −30 °C), in which external selective oxidation of Mn and Si is favored, were chosen as typical low DP atmospheres. These low DP conditions are close to the actual atmosphere of the annealing furnace in industrial lines. The gas atmospheres with DPs of 273 K and 278 K (0 °C and +5 °C), in which internal selective oxidation of Mn and Si is favored, were chosen as high DP atmospheres. The gas atmosphere with a DP of 263 K (−10 °C), where the transition from external to internal oxidation was observed in a previous study,^[15] was chosen as an intermediate DP atmosphere. The oxygen partial pressure at each DP condition listed in Table I was calculated using the formulae given by Huin *et al.*^[16]

Prior to the galvannealing simulation, the sheets were degreased with kerosene and ultrasonically cleaned in ethanol and acetone to remove all lubricant residues and iron fines. The galvannealing cycle consisted of heating with a heating rate of 3 K/s to the IA temperature of 1093 K (820 °C). The panels were held at the IA temperature for 47 seconds, slow cooled with a cooling rate of 3 K/s to 943 K (670 °C), rapidly cooled with a cooling rate of 17.6 K/s to the isothermal bainitic transformation (IBT) temperature of 673 K (400 °C), held at the IBT temperature for 120 seconds, dipped in the Zn bath for 4 seconds, and immediately reheated to the galvannealing temperature with a heating rate of 17 K/s prior to a final rapid cooling to room temperature with a cooling rate of 20 to 30 K/s. The Zn bath temperature was 733 K (460 °C) and the total Al content of the Zn was 0.13 mass pct. The Al content in the bath was selected to induce the formation of a

Table I. Oxygen Partial Pressure at an IA Temperature of 1093 K (820 °C) as a Function of the Gas Atmosphere DPs

DP [K (°C)]	Oxygen Partial Pressure at IA Temperature 1093 K (820 °C) in a N ₂ + 10 pct H ₂ Gas Atmosphere (atm)
213 (−60)	1.29×10^{-26}
243 (−30)	1.58×10^{-23}
263 (−10)	7.38×10^{-22}
273 (0)	4.09×10^{-21}
278 (+5)	8.33×10^{-21}

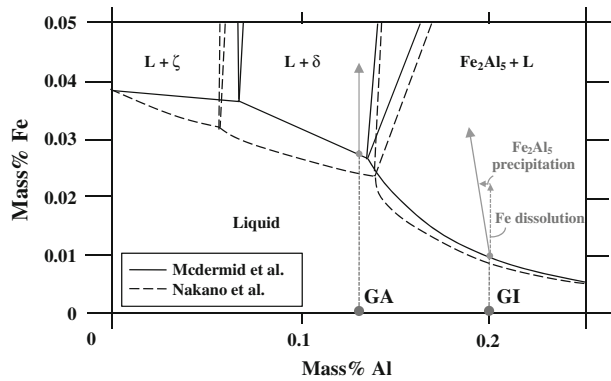


Fig. 1—733 K (460 °C) isothermal section of the Zn-rich corner of the Zn-Al-Fe phase diagram. The arrows indicate the direction of the shift of the local bath composition at the steel/coating interface when Fe dissolves into the liquid Zn during the hot dipping. The Al content of the Zn baths is indicated by the points labeled GI and GA for galvanizing and galvannealing, respectively. The phase diagrams suggested by Mcdermid *et al.*, and Nakano *et al.*,^[17,18] were used.

layer of δ phase crystals and minimize the formation of the $\text{Fe}_2\text{Al}_5\text{-xZn}_x$ inhibition layer or ζ phase crystal. The 733 K (460 °C) isothermal section of the Zn-Al-Fe diagram of Figure 1 shows the shift of the local bath composition near the steel/coating interface from its original alloy content, *i.e.*, Zn with 0.13 mass pct Al, to the L + δ region by Fe dissolution during the hot dipping.^[17,18] Although the galvannealing temperatures of the simulations were programmed to be 843 K (570 °C), the actual temperature varied in the range of 813 K to 844 K (540 °C to 571 °C) because the precise control of the galvannealing temperature was difficult due to the characteristics of the induction heating equipment. The actual galvannealing temperatures of the samples annealed in gas atmospheres with DPs of 213 K, 243 K, 263 K, 273 K, and 278 K (−60 °C, −30 °C, −10 °C, 0 °C, and +5 °C) were 813 K, 824 K, 844 K, 841 K, and 821 K (540 °C, 551 °C, 571 °C, 568 °C, and 548 °C), respectively.

The surface and cross section of the GA samples were analyzed in a FE-EPMA operated at 15 keV using a 50-nA beam current. The cross section of the GA samples was mirror polished with a 1 μm diamond suspension prior to the EPMA observation. The samples were analyzed in a JEOL JXA-8530F FE-EPMA. The microstructure characterization of the GA samples was carried out in a TEM. The cross-sectional TEM samples were prepared by the FIB technique in an FEI Quanta 3D FEG. The TEM samples were analyzed in a JEOL JEM-2100 TEM and a JEOL JEM-2100F FE-TEM operated at 200 keV. The composition of the oxides and Fe-Zn intermetallic phases was determined by means of energy dispersive spectroscopy (EDS) using a one nanometer-sized electron beam.

III. RESULTS

Figure 2 shows pictures of GA TRIP steel panels annealed in a gas atmosphere with DPs of 213 K and

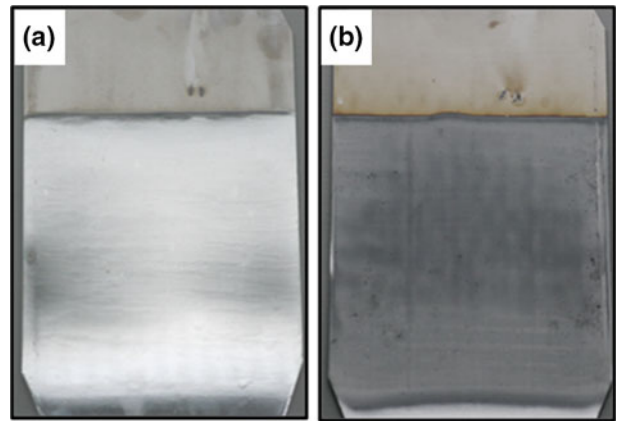


Fig. 2—GA panels of CMnSi TRIP steel intercritically annealed in a gas atmosphere with a DP of (a) 213 K (−60 °C) and (b) 278 K (+5 °C).

278 K (−60 °C and +5 °C). Despite the similar galvannealing temperatures, the coating quality of the GA panels was significantly different for the two panels. The coating of the panel annealed in the low DP conditions was not fully GA, and its surface still consisted of metallic Zn. In contrast, the coating on the panel annealed in a high DP [278 K (+5 °C)] gas atmosphere was fully alloyed.

Figure 3 shows SEM micrographs and FE-EPMA elemental maps for Fe, Zn, and Al of the surface of the GA TRIP steels. The coating surface on the panel annealed in a low DP [213 K (60 °C)] gas atmosphere had coarse δ phase crystals with a polygonal morphology embedded in η phase crystals. Higher Fe and Al contents and a lower Zn content were measured for the δ phase crystals. The coating surface on the panel annealed in an intermediate DP [263 K (−10 °C)] gas atmosphere had two types of δ phase crystals: coarse δ phase crystals and fine δ phase crystals. The coating surface on the panel annealed in a high DP [278 K (+5 °C)] gas atmosphere also had the same types of δ phase crystals. A majority of the crystals in the coating layer were fine δ phase crystals. Higher Fe and Al contents and a lower content of Zn were detected in the fine δ phase crystals compared to the coarse δ phase crystals. Annealing in a higher DP gas atmosphere resulted in a higher concentration of Fe and Al at the coating surface.

Figure 4 shows SEM micrographs and FE-EPMA elemental maps for Fe, Zn, Al, Mn, and Si of the cross section of the coating layer of the GA TRIP steels. In parts of the coating layer of the panel annealed in a low DP gas atmosphere, δ phase crystals were observed, but in other parts of the coating layer, η phase crystals remained present, as shown in Figure 4(a). Al was enriched at the steel/coating interface. The arrows in the Mn elemental map indicate that the $x\text{MnO}\cdot\text{SiO}_2$ oxides formed during IA were mostly located near the steel/coating interface. The coating layer on the panel annealed in an intermediate DP gas atmosphere consisted of two types of δ phase crystals. The upper part of the coating layer consisted mainly of coarse δ phase crystals. The lower coating layer consisted of compact and fine δ phase crystals. The detailed microstructure of

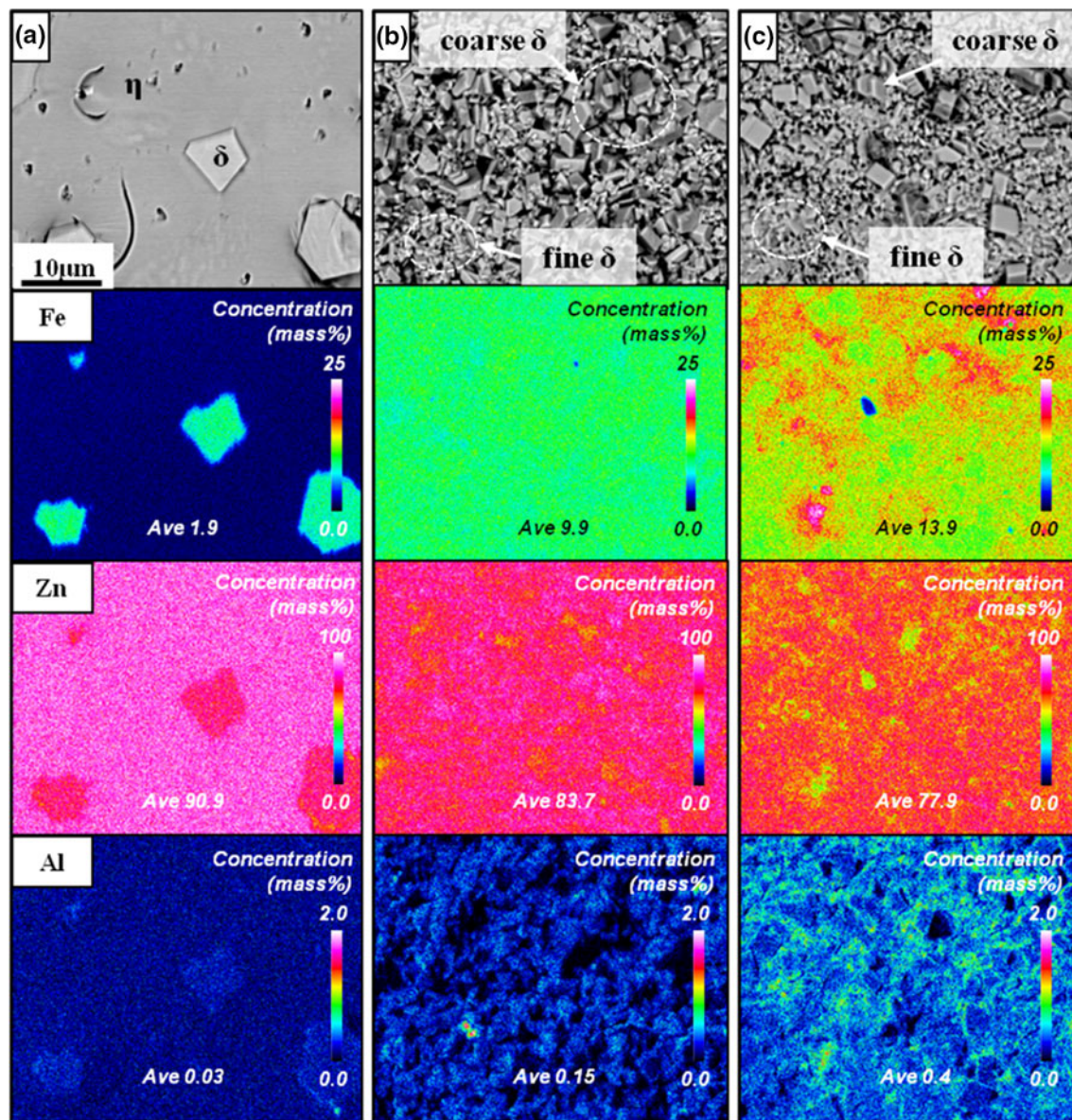


Fig. 3—SEM micrographs and FE-EPMA elemental mapping images for Fe, Zn, and Al on the coating surface of the GA TRIP steels. The steel was annealed in the following DP conditions: (a) 213 K (−60 °C), (b) 263 K (−10 °C), and (c) 278 K (+5 °C).

these coarse and fine δ phase crystals will be described in the paragraphs related to the TEM results. The Fe content was slightly higher in the lower coating layer. Al and the $x\text{MnO}\cdot\text{SiO}_2$ oxides formed during IA were located below the coarse δ phase crystals of the upper part of the coating layer. The coating layer on the panel annealed in a high DP gas atmosphere consisted mainly of fine δ phase crystals. A layer of Γ phase crystals was present at the steel/coating interface. Al was mostly present at the surface of the coating layer. The $x\text{MnO}\cdot\text{SiO}_2$ oxides formed during the IA were distributed throughout the coating layer. Annealing in a higher DP gas atmosphere resulted in the formation of a compact layer of δ phase crystals and a layer of Γ phase crystals at the steel/coating interface.

Figure 5 shows cross-sectional TEM micrographs of the coating layer on the GA TRIP steel annealed in a

low DP [213 K (−60 °C)] gas atmosphere. Figure 5(a) shows a STEM dark field (DF) micrograph of the coating layer consisting of η phase crystals and a single crystal of δ phase. Note that the layer covering the sample surface is a Pt coating layer which was deposited to protect the surface during the FIB sample preparation. The gap with dark contrast between the δ phase crystal and the η phase crystal is a void created during the FIB milling. No oxides were observed in the coating layer of the TEM sample. The oxides were present in the vicinity of the steel/coating interface. Figure 5(b) shows a bright field (BF) image of the η phase crystal. The 0.239-nm inter-planar distance of the (010) $_{\eta}$ lattice planes is indicated in the corresponding diffraction pattern in Figure 5(c). Figure 5(d) shows a diffraction pattern of the single crystal of the δ phase. The 0.217-nm inter-planar distance of the ($\bar{3}60$) $_{\delta}$ lattice planes is

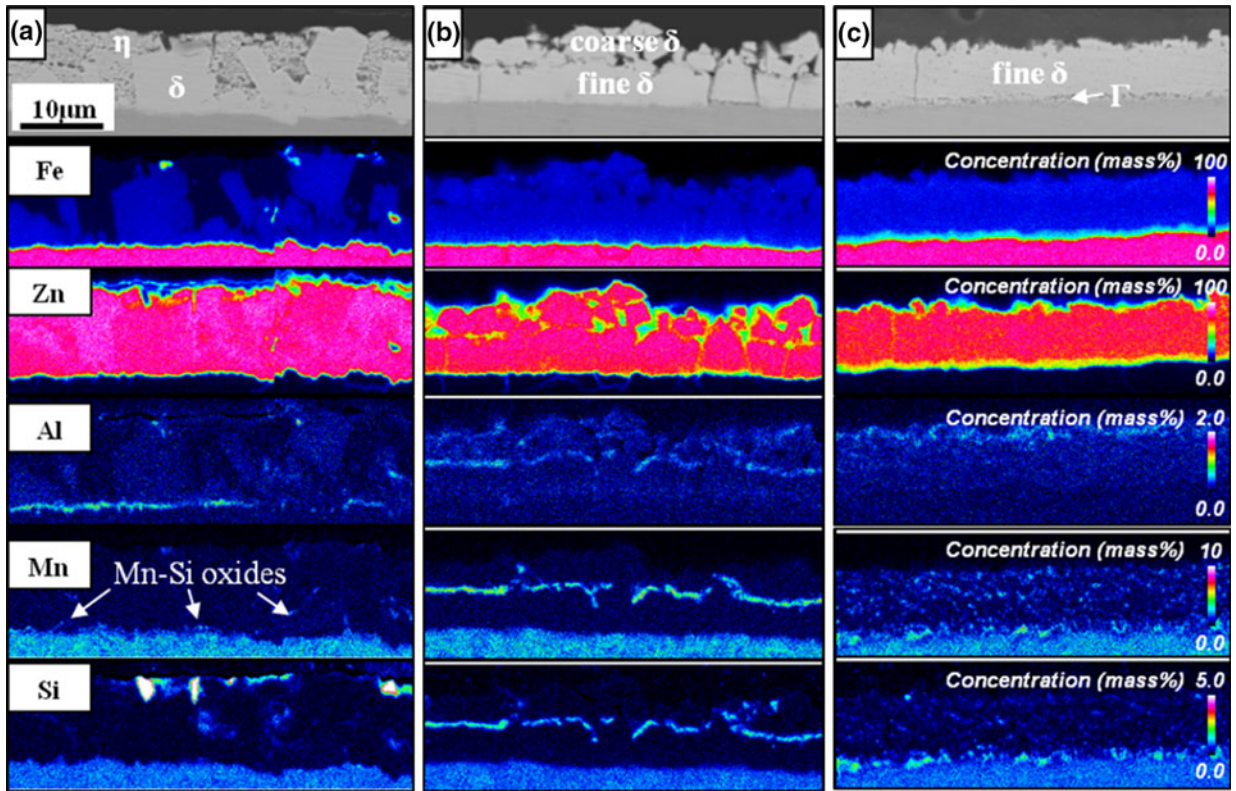


Fig. 4—SEM micrographs and the FE-EPMA elemental mapping images for Fe, Zn, Al, Mn, and Si of the coating layer on the GA TRIP steel. The steel was annealed in the following DP conditions: (a) 213 K (−60 °C), (b) 263 K (−10 °C), and (c) 278 K (+5 °C).

indicated. The Fe content near the top surface of the δ phase crystal was in the range of 9–10 mass pct.

Figure 6 shows cross-sectional TEM micrographs of the coating layer on the GA TRIP steel annealed in a low DP [243 K (−30 °C)] gas atmosphere. Figure 6(a) shows an overview TEM micrograph of the alloy layer, which consisted of δ phase crystals. The empty space with a bright contrast is a hole created during FIB milling. The gap area is located where η phase crystals were present as pure Zn is easily removed during FIB milling. Part of a ferrite grain can be seen embedded in the δ phase crystals. Most of the oxides were present near the steel/coating interface. The Fe content near the surface of the coating layer was 10.1 mass pct. Figure 6(b) shows a TEM image of oxides with a spherical shape present near the steel/coating interface. Figure 6(c) shows an enlarged image and the EDS spectrum of the oxides. The EDS spectrum shows that the oxides were complex Mn-Si-Al ternary compound oxides. Most of the oxides observed near the steel/coating interface contained Al. This indicates that the Mn-Si compound oxides formed during IA were changed to Mn-Si-Al oxides by reaction with Al dissolved in the Zn bath. Figure 6(d) shows a fine δ phase crystal which has grown on a ferrite grain. Figure 6(e) shows the diffraction pattern and the EDS spectrum of the δ phase crystal. The 1.113-nm inter-planar distance of the $(01\bar{1}0)_\delta$ lattice planes is indicated. The Fe content of the δ phase crystal was 10.3 mass pct. Figure 6(f) shows the δ phase crystals present between ferrite grains. δ phase crystals were also present at the ferrite grain

boundaries. The Zn atoms appeared to have been penetrated through the ferrite grain boundaries. This strongly suggests that the grain boundary diffusion is significantly faster than the lattice diffusion. Shewmon *et al.*^[19] have studied the rate of diffusion of Zn into Fe in solid Fe/Zn diffusion couple and reported that the Zn diffusion in ferrite was anomalously faster than would be predicted by lattice diffusion. Dohie *et al.*^[20] subsequently argued that the fast Zn diffusion in ferrite was due to the contribution of Zn grain boundary diffusion. They showed that if both lattice diffusion and grain boundary diffusion contributed to mass transport, the diffusion rate of Zn in ferrite was similar to the diffusion rate in other polycrystalline metals. The observation of the Zn penetration into the ferrite grain boundaries in Figure 6(f) supports this view.

Figure 7 shows a cross-sectional SEM micrograph of the interface between the coarse δ phase crystals of the top part of the coating layer and the fine δ phase crystals of the lower part of the coating layer. The oxides with a dark contrast, formed during IA, were clearly present at the interface, as indicated by the arrow in Figure 7. Previous work has shown that IA of TRIP steel in a gas atmosphere with a DP of 263 K (−10 °C) resulted in the internal selective oxidation of Mn and Si with an oxidation front depth of ~500 nm.^[15] The morphology of the internal oxides observed after IA was very similar to the morphology of the oxides observed after galvannealing. However, after galvannealing, the oxides were located between the coarse δ phase crystals of the upper part of the coating layer and the fine δ phase crystals of

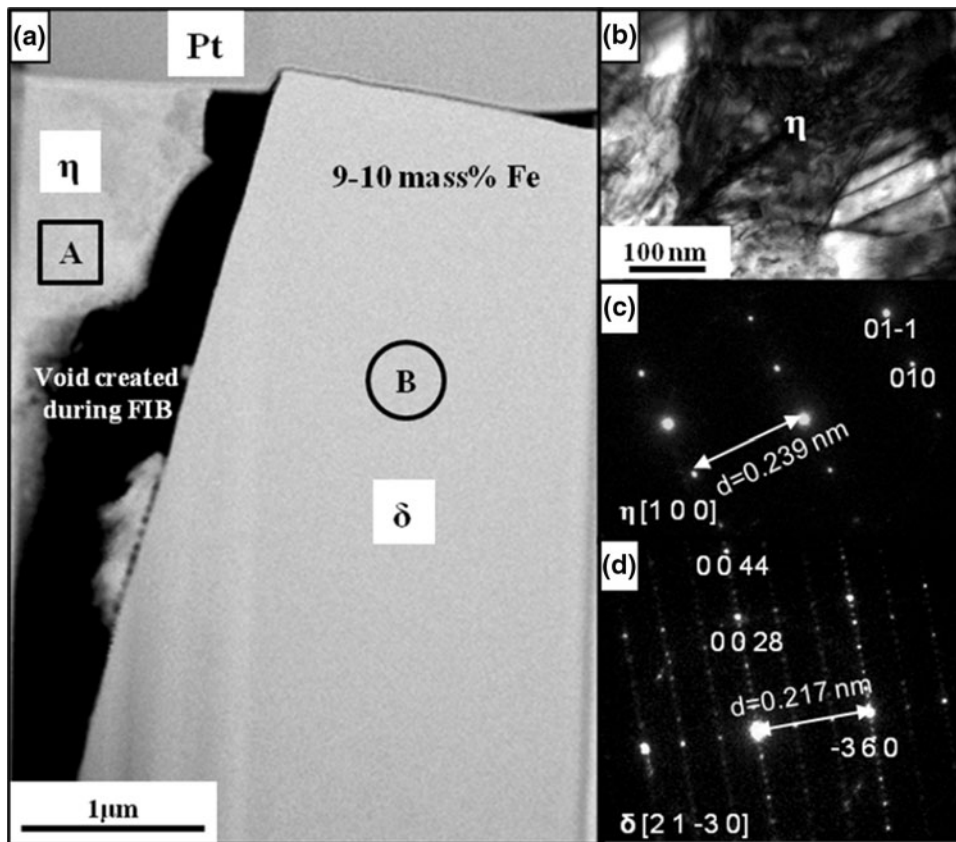


Fig. 5—Cross-sectional FE-TEM micrographs of the GA coating layer on CMnSi TRIP steel intercritically annealed in a low DP gas atmosphere of 213 K (−60 °C). (a) Overview STEM DF micrograph of the coating layer. (b) TEM BF image of the enlarged area corresponding to A in (a). (c) Diffraction pattern of η phase in (b). (d) Diffraction pattern of δ phase in (a).

the lower part of the coating layer. The growth of the Fe-Zn crystals displaced the $x\text{MnO}\cdot\text{SiO}_2$ oxides and they then moved the oxides away from their original position during the galvannealing process. The dispersion of the oxide by the Fe-Zn interdiffusion was also observed in the previous study.^[15]

Figure 8 shows cross-sectional TEM micrographs of the coating layer on the GA TRIP steel annealed in an intermediate DP [263 K (−10 °C)] gas atmosphere. Figure 8(a) shows a STEM DF micrograph of an overview of the coating layer. The coating layer consisted of δ phase crystals and a thin layer of Γ phase crystals. The grain size of the δ phase crystals was larger in the upper part of the coating layer in comparison to the lower part of the coating layer. The Fe content near the surface of the coating layer was in the range of 9 to 10 mass pct. $x\text{MnO}\cdot\text{SiO}_2$ oxides with a dark contrast were present at mid thickness in the coating layer, as indicated by the arrow in Figure 8(a). Figure 8(b) shows a detailed view of the steel/coating interface. A layer of Γ phase crystals was present at the steel/coating interface. It had a thickness in the range of 50 to 300 nm. Figure 8(c) shows a diffraction pattern and an EDS spectrum of the steel matrix. The steel matrix was ferritic with close to 100 mass pct Fe. The previous studies^[15] on the selective oxidation of the intercritical annealed TRIP steel have also shown that only ferrite grains were observed near the surface. Both retained austenite and

martensite were absent near the surface of the TRIP steels because the steel surface is decarburized during the annealing and Mn, an austenite stabilizer, is subject to selective oxidation during annealing. Liu *et al.*^[21] also reported that since the surface of a TRIP steel was decarburized during annealing, a 20- μm -thick ferrite layer was formed near the strip surface. Figure 8(d) shows a diffraction pattern and the EDS spectrum of a Γ phase crystal present at the steel/coating interface. An inter-planar spacing of 0.465 nm was measured for the (0 2 0) Γ lattice planes. The Fe content of the Γ phase crystal was 28.8 mass pct. Occasionally, Γ_1 phase crystals were also observed at the Γ/δ interface. The Fe content in the Γ_1 phase crystal was 17.3 mass pct, as calculated from the EDS spectrum of Figure 8(e).

Figure 9 shows cross-sectional TEM micrographs of the coating layer on the GA TRIP steel annealed in a high DP [273 K (0 °C)] gas atmosphere. Figure 9(a) shows a TEM micrograph of the coating layer consisting of δ phase crystals and a thin layer of Γ phase crystals. The grain size of the δ phase crystals in the lower part of the coating was smaller than in the upper part of the coating layer. The Fe content was higher in the fine-grained δ phase crystals. The Fe content was 15.7 mass pct in the fine δ phase crystals and 10 to 11 mass pct in the coarse δ phase crystal. While the $x\text{MnO}\cdot\text{SiO}_2$ oxides were distributed homogeneously throughout the entire coating, they were not present in the area of the coarse δ

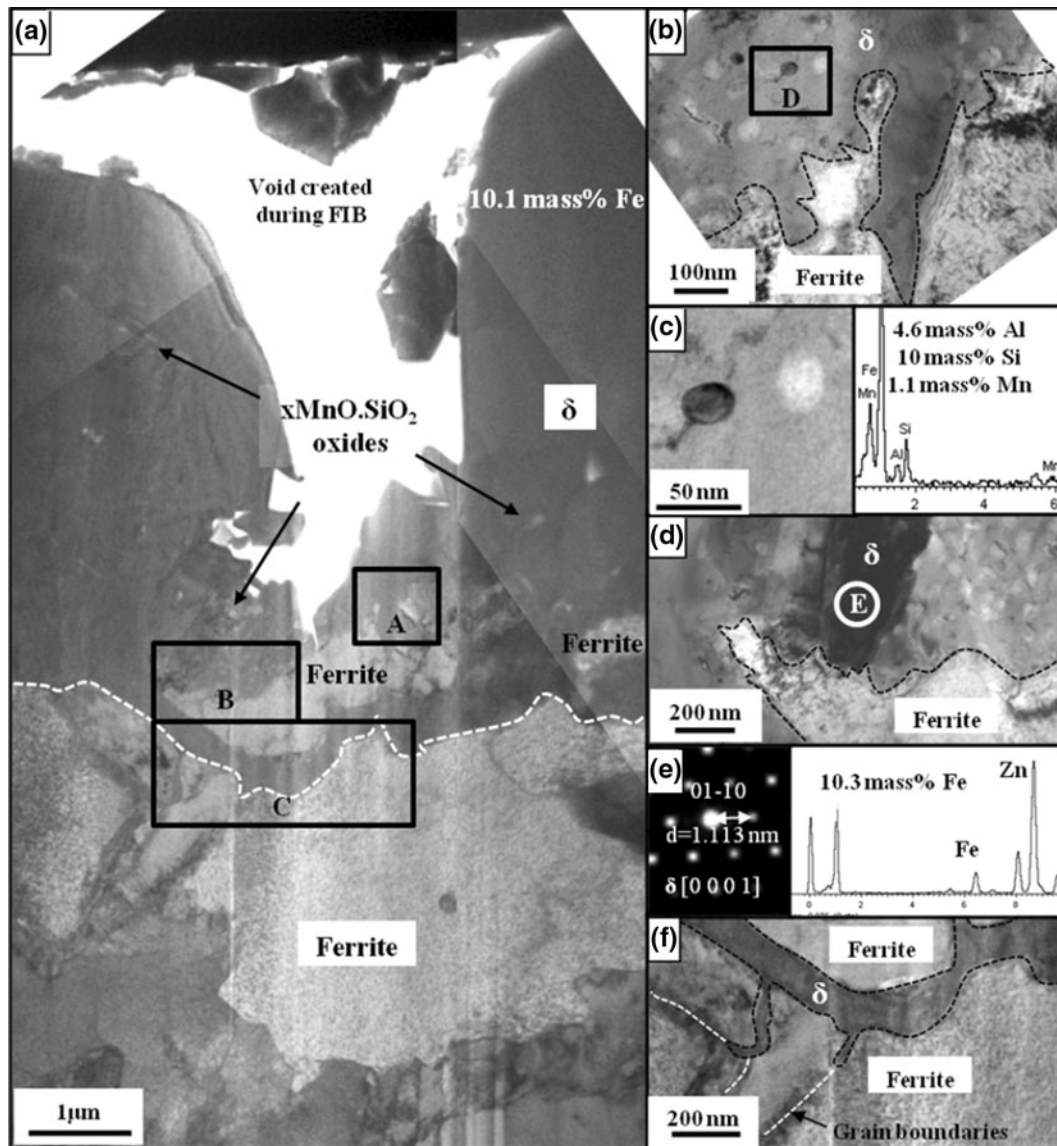


Fig. 6—Cross-sectional TEM micrographs of the GA coating layer on CMnSi TRIP steel intercritically annealed in a low DP gas atmosphere of 243 K (−30 °C). (a) Overview TEM micrograph of the coating layer. (b) Enlarged area of the steel/coating interface corresponding to A in (a). (c) TEM image of the enlarged area of the Mn-Si-Al compound oxides embedded in the δ crystal corresponding to D in (b) and an EDS spectrum of the Mn-Si-Al oxide. (d) TEM BF image of the enlarged area of the δ phase crystals corresponding to B in (a). (e) Diffraction pattern and an EDS spectrum of E in the δ phase crystals in (d). (f) TEM image of the enlarged area corresponding to C in (a) showing δ phase crystals present under the ferrite grains.

phase crystals of the upper part of the coating layer. Figure 9(b) shows a detailed view of the steel/coating interface. A layer of the Γ phase crystals was present at the steel/coating interface. It had a thickness of 1.0 to 1.2 μm . Figure 9(c) through (e) shows diffraction patterns and EDS spectra of the steel matrix, the Γ phase, and the δ phase.

Figure 10 shows TEM micrographs of the coating layer on the GA TRIP steel annealed in a high DP [278 K (+5 °C)] gas atmosphere. The microstructure of the coating layer was in general very similar to the one of the sample annealed in a DP [273 K (0 °C)] condition (Figure 9), particularly with respect to the morphology of the δ phase crystals and the distribution of the $x\text{MnO}\cdot\text{SiO}_2$ oxides. Figure 10(a) shows a STEM DF

micrograph of the coating layer, which consisted of δ phase crystals and a thin layer of Γ phase crystals. The morphologies of the δ phase crystals present in the upper part and the lower part of the coating layer were clearly different. The δ phase crystals of the upper part of the coating layer had a polygonal morphology, whereas the δ phase crystals of the lower part of the coating layer had a columnar morphology. The columnar δ phase crystals grew vertically from the steel/coating interface. Similar to the GA steel sample annealed in a DP of 273 K (0 °C), fine-grained δ phase crystals with a higher Fe content were present in the lower part of the coating layer and coarse-grained δ phase crystals with a lower Fe content were present at the upper part of the coating layer. This observation is

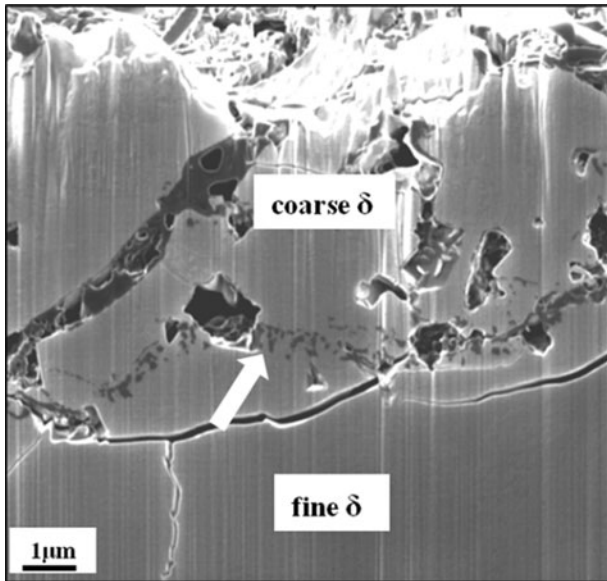


Fig. 7—Cross-sectional SEM micrograph of the GA coating layer on CMnSi TRIP steel intercritically annealed in an intermediate DP gas atmosphere of 263 K (-10°C). The arrow indicates the internal and external oxides embedded in the δ layer after the Fe-Zn reaction.

in agreement with the result of the higher Fe content measured for the fine δ crystals by EPMA analysis [Figure 3(c)]. The oxides were homogeneously distributed within the coating layer, but they were not present in the coarse δ phase crystals. Figure 10(b) shows that Mn-Si-Al ternary compound oxides were present near the coating surface. The position of the oxides present in the δ crystal was strongly altered by the growth of the δ phase crystals. Many oxides were observed at the grain boundaries of the δ phase crystals, as shown in Figure 10(c). This observation reveals that the oxides were clearly displaced by the growth of the δ phase crystals. The δ phase crystals were identified by selected area electron diffraction as shown in Figure 10(c). The 1.174-nm interplanar spacing of the $(0110)_{\delta}$ lattice planes is indicated in the diffraction pattern. Figure 10(d) shows a TEM BF micrograph of the fine δ phase crystals of which the grain boundaries were clearly visible. There was no compositional difference between the fine δ phase crystals. Figure 10(e) shows a detailed view of the Γ phase crystals present at the steel/coating interface [area D in Figure 10(a)]. The thickness of the layer of the Γ phase crystals was 1.0 to 1.2 μm . The diffraction pattern of the Γ phase of Figure 10(e) is shown in Figure 10(f). The interplanar spacing of 0.644 nm was measured for the $(01\bar{1})_{\Gamma}$ lattice planes. The corresponding diffraction pattern of the ferrite phase is shown in Figure 10(g). Only ferrite was observed in the steel as a result of decarburization. No crystallographic orientation relationship between the Γ phase crystal and the ferrite was observed. Note that the lower part of the ferrite region with a brighter contrast in Figure 10(a) is the edge of the TEM sample damaged during FIB milling.

Figure 11 shows a STEM image of the area labeled D in Figure 10(a) and an EDS elemental profile of the steel/coating interface which includes ferrite, a Γ phase

crystal, and δ phase crystals. The EDS elemental composition was taken along the dashed line in the direction of the arrow in Figure 11(c). The oxides near the steel/ Γ interface were not influenced by the Fe-Zn interdiffusion. The oxides had the same characteristic dendritic morphology of the internal oxides observed prior to hot dipping.^[15] The Γ phase crystal contained 23 to 28 mass pct Fe and the δ phase crystal contained 14 to 15 mass pct Fe. The Fe content was slightly higher on the ferrite side of the Γ phase crystal than on the δ phase crystal side. The EDS result indicates that no Γ_1 phase crystals were present at the Γ/δ interface.

IV. DISCUSSION

Due to its technological importance, the Zn-rich corner of the Fe-Zn-Al phase diagram and the Fe-Zn intermetallic phases have been the subject of a large number of research reports.^[22–26] Table II reviews the available crystallographic and compositional information for the Fe-Zn phases ζ , δ , Γ_1 , and Γ . The δ phase forms in two morphologies: the palisade morphology and the compact morphology.^[2,27] The palisade morphology δ (δ_p) phase and the compact morphology δ (δ_k) phase have the same crystallographic structure, but a different appearance and composition. The δ_p phase crystals are formed at the Zn-rich side of the coating layer. A strong fiber texture has been reported for δ_p phase crystals, with the $(10\bar{1}0)$ or $(11\bar{2}0)$ type planes of the hexagonal δ_p oriented parallel to the steel/coating interface.^[28,29] This implies that the basal planes are perpendicular to the steel/coating interface, as shown in Figure 12. The δ_k phase crystals are formed on the Fe-rich side of the coating layer. In the present study, the Fe-Zn intermetallic phase crystals observed at the GA coating layer were mostly the δ and Γ phase. ζ phase crystals were not observed and the Γ_1 phase was rarely observed at the Γ/δ interface. The reason for these observations is the fast rate of heating (17 K/s) from the Zn bath temperature [733 K (460 $^{\circ}\text{C}$)] to the relatively high galvannealing temperature [813 K to 843 K (540 $^{\circ}\text{C}$ to 570 $^{\circ}\text{C}$)] where the δ and Γ phases are thermodynamically stable.^[30] The δ phase crystals observed in the present study were all identified as being δ_p phase crystals. Although δ phase crystals with a polygonal morphology have occasionally been observed in the present study [Figures 9(a) and 10(a)], they are different from the δ_k phase crystal identified in the past in two aspects. First, they were not present at the Fe-rich side, but at the Zn-rich side of the δ phase layer. Second, they were formed during galvannealing for very short time (5 to 10 s), while the δ_k phase crystal identified in previous reports was only formed after prolonged annealing.^[27,31,32] The polygonal morphology of the δ phase crystals observed in the present study is due to the two-stage growth process of δ_p phase crystals. First, coarse δ_p phase crystals are formed and grow and, subsequently, the fine δ_p phase crystals are formed from the steel/coating interface. As the fine δ_p phase crystals grow, the lower part of the coarse δ_p phase crystals appears to be removed. The remaining δ_p phase crystals

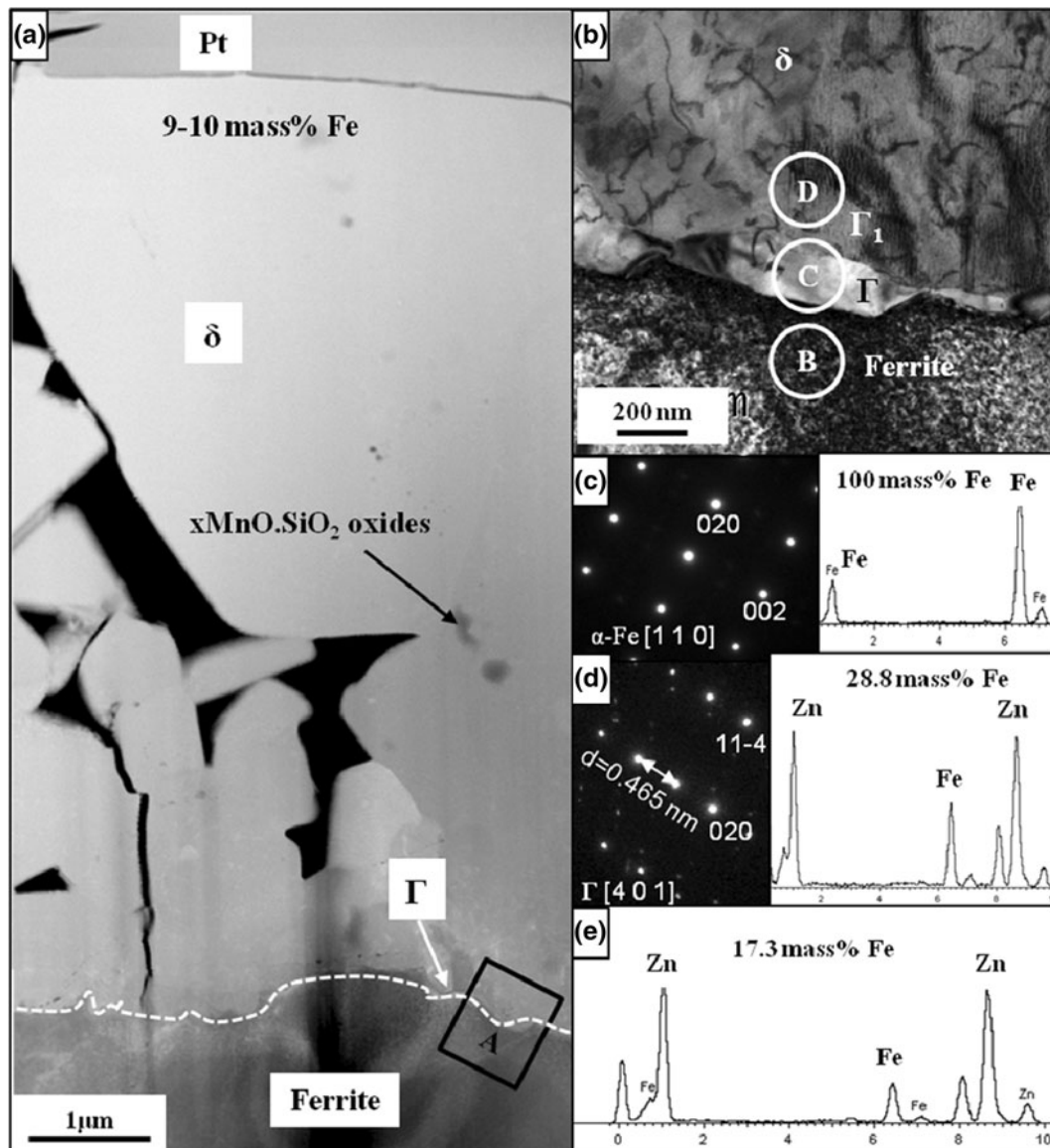


Fig. 8—Cross-sectional FE-TEM micrographs of the GA coating layer on CMnSi TRIP steel intercritically annealed in an intermediate DP gas atmosphere of 263 K (−10 °C). (a) Overview STEM DF micrograph of the coating layer. (b) TEM BF image of the enlarged area of the steel/coating interface corresponding to A in (a). (c) Diffraction pattern and EDS spectrum of B in the ferrite region in (b). (d) Diffraction pattern and EDS spectrum of C in the Γ phase region in (b). (e) EDS spectrum of D in the Γ_1 phase region in (b).

at the surface side of the coating are polygonal. The mechanism for this two-step growth process will be described in detail in the discussion as will the origin of texturing of the δ_p phase crystals.

As the annealing furnace of the gas atmosphere DP determines the oxygen partial pressure, the control of the gas atmosphere DP allows for internal oxidation of Mn and Si rather than external oxidation during the IA. When the external oxides, which act as obstacles to the diffusion of Fe and Zn during galvannealing, do not form a continuous layer, the Fe-Zn reaction is expected to proceed rapidly. Thus, annealing in a gas atmosphere with a high DP will result in internal oxidation and lead to an acceleration of the galvannealing reaction.^[5,6]

The experimental results of the present study show the effectiveness of the use of a higher annealing furnace gas

atmosphere DP to improve the formation of the Zn-alloy coating on Si-alloyed TRIP steel. A previous study^[15] on the selective oxidation during IA of the CMnSi TRIP steel has shown that morphology, type, and layer thickness of the surface oxides were significantly different depending on DP gas atmosphere. In a low DP [213 K (−60 °C)] gas atmosphere, two types of surface oxides were formed on the surface during IA: thick (30 to 40 nm) $x\text{MnO}\cdot\text{SiO}_2$ ($1 < x < 5$) layers and thin (5 to 10 nm) $\alpha\text{-SiO}_2$ layers. Annealing in the higher DP [263 K and 278 K (−10 °C and +5 °C)] gas atmospheres resulted in a thinner layer of external oxidation and a larger depth of internal oxidation. In a high DP [278 K (+5 °C)] gas atmosphere, a thin (5 to 15 nm) $x\text{MnO}\cdot\text{SiO}_2$ ($1 < x < 2$) layer was formed on the surface, and particle-type oxides were present at the

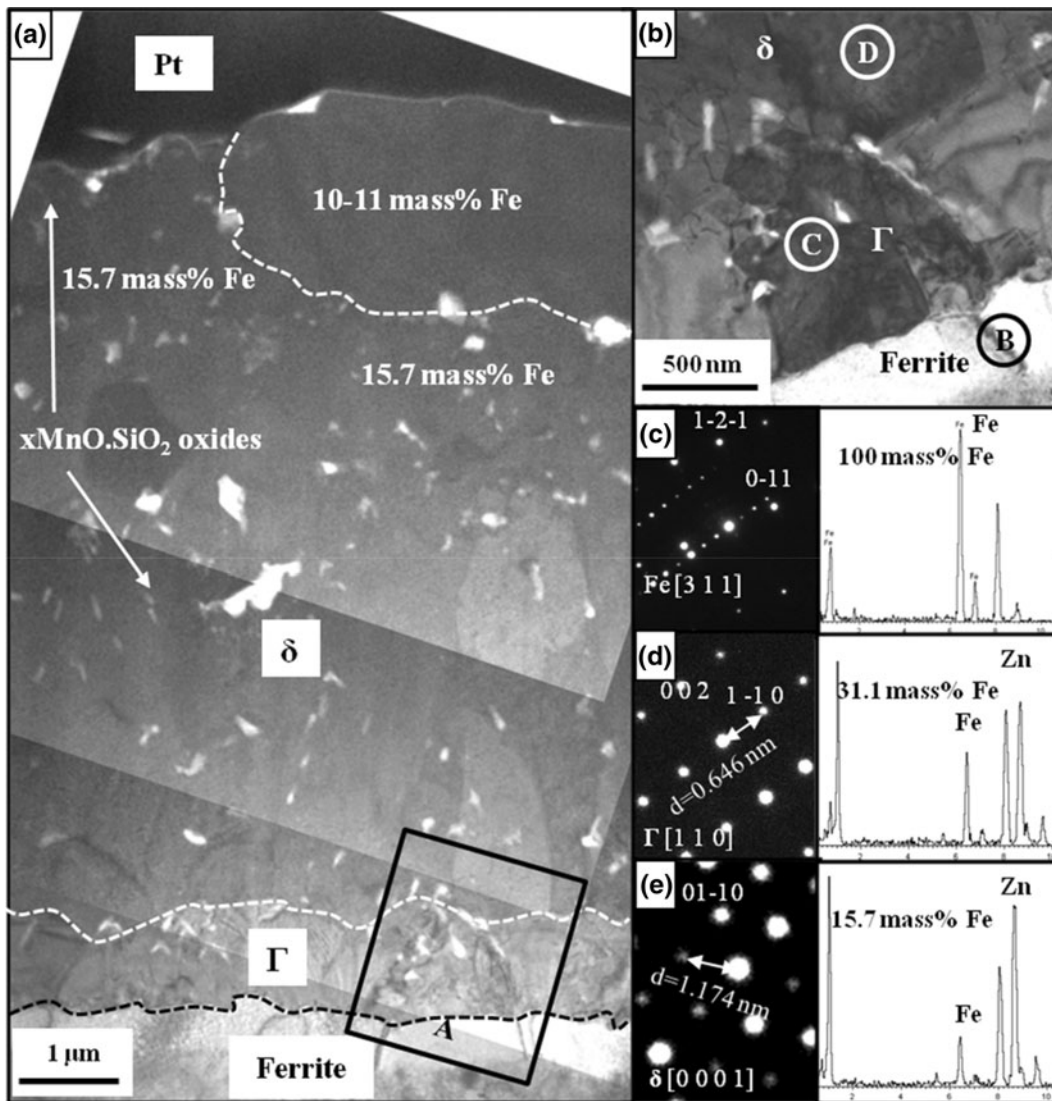


Fig. 9—Cross-sectional TEM micrographs of the GA coating layer on CMnSi TRIP steel intercritically annealed in a high DP gas atmosphere of 273 K (0 °C). (a) Overview TEM micrograph of the coating layer. (b) Enlarged area of the steel/coating interface corresponding to A in (a). (c) Diffraction pattern and EDS spectrum of B of the ferrite region in (b). (d) Diffraction pattern and EDS spectrum of C of the Γ phase region in (b). (e) Diffraction pattern and EDS spectrum of D of the δ phase region in (b).

surface of ferrite grain boundaries. $x\text{MnO}\cdot\text{SiO}_2$ ($0 < x < 2$) oxides were formed in the subsurface. The depth of internal oxidation ranged from 1.0 to 1.2 μm .

The present work shows that only the panels processed in high DP gas atmospheres were fully GA during galvannealing. η and δ phase crystals were present in the coating on the panels intercritically annealed in low DP [213 K and 243 K (−60 °C and −30 °C)] conditions, whereas δ and Γ phase crystals were observed at the coating layer of the panels intercritically annealed in the intermediate DP [263 K (−10 °C)] and high DP [273 K and 278 K (0 °C and +5 °C)] gas atmospheres. The Fe content of the coating layers also increased after annealing in gas atmospheres with a higher DP. It should be pointed out that, in spite of the fact that the galvannealing temperature of the panel intercritically annealed in the high DP [278 K (+5 °C)] condition was lower than that of the panel intercritically annealed in

the intermediate DP [263 K (−10 °C)] condition, the average Fe content in the coating of the panel annealed in the high DP condition was higher. Galvannealing in the presence of a thinner external oxide layer therefore resulted in faster kinetics for the Fe-Zn reaction.

In order for the galvannealing reaction to take place in the presence of an oxide layer, the oxide layer must be broken down by the physical penetration of Fe or Zn through defects in the oxide layer. The penetration is much slower than normal lattice diffusion in steel because the surface oxide layers are often amorphous and continuous. Therefore, when the surface oxide layers are thicker, the initiation of the Fe-Zn reaction takes much more time as Fe and Zn must penetrate through and break down a dense oxide layer.

The faster kinetics of the Fe-Zn reaction during the galvannealing of panels intercritically annealed in high DP gas atmospheres affected the distribution of Al and

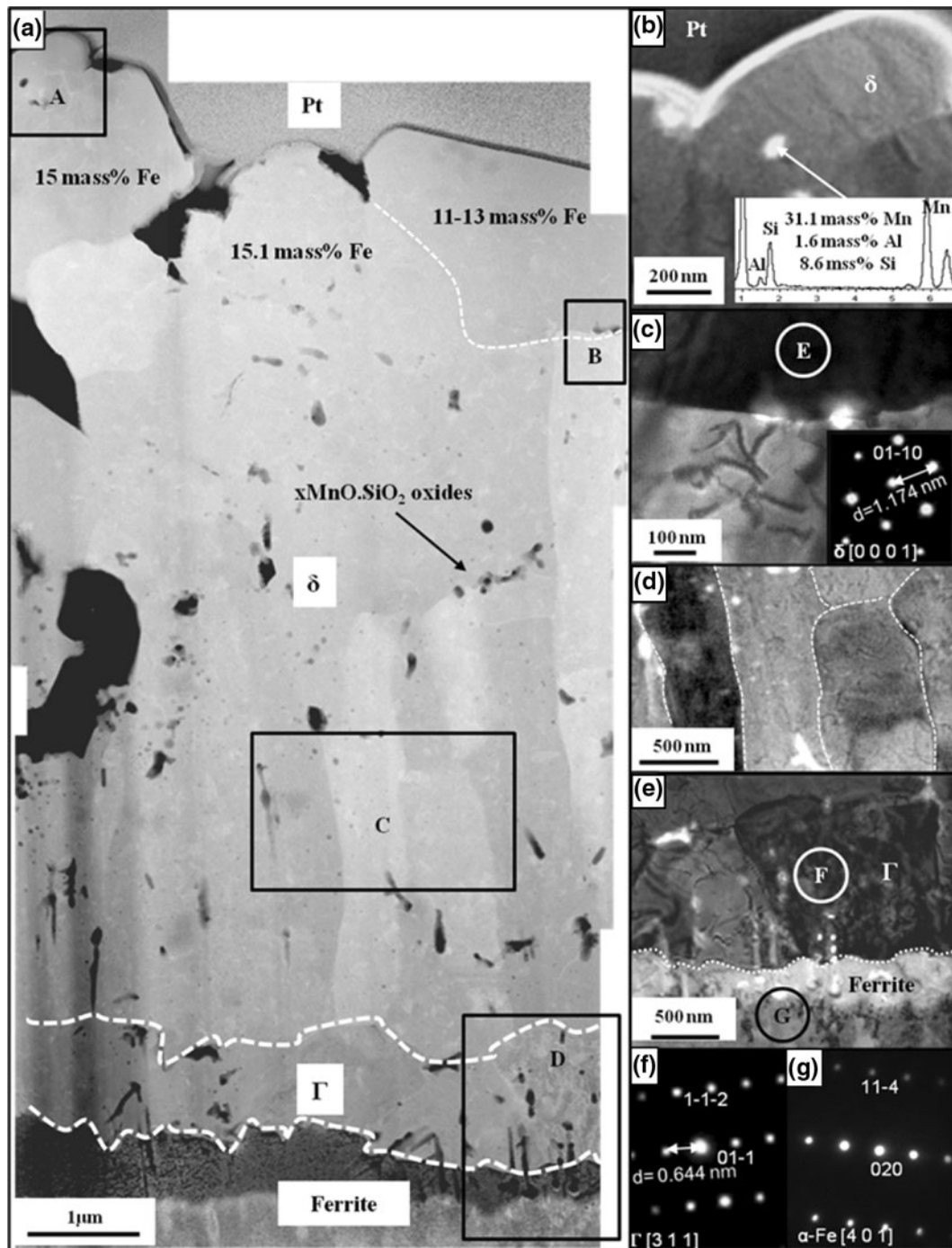


Fig. 10—Cross-sectional FE-TEM micrographs of the GA coating layer on CMnSi TRIP steel intercritically annealed in a high DP gas atmosphere of 278 K (+5 °C). (a) Overview STEM DF micrograph of the coating layer. (b) Enlarged area of the surface of the coating layer corresponding to A in (a). EDS spectrum indicating that the Mn-Si compound oxide present near the surface of the δ crystal coating layer contains Al. (c) TEM BF image of the enlarged area of the grain boundary of δ phase crystals corresponding to B in (a). Diffraction pattern of D used for identification of the δ phase crystals. (d) TEM BF image of the enlarged area of the fine δ phase crystals corresponding to C in (a). (e) TEM BF image of the enlarged area of the steel/coating interface corresponding to D in (a). (f) Diffraction pattern of E in the Γ phase region in (e). (g) Diffraction pattern of F in the ferrite region in (d).

the oxides in the GA coating layer. Coarse δ phase crystals formed during the galvannealing of panels intercritically annealed in low DP gas atmospheres contained 9 to 10 mass pct Fe (Figures 5, 6). Al and the $x\text{MnO}\cdot\text{SiO}_2$ oxides were present near the steel/coating interface [Figures 4(a) and 6(a) through (c)]. Despite the

fact that 0.13 mass pct Al in the Zn bath is thermodynamically insufficient to form Fe_2Al_5 inhibition layer,^[17] Al was locally enriched and formed a thin Fe_2Al_5 layer at the steel/coating interface during the hot dipping. Baril and L'Esperance^[33] observed this Al-rich layer at the steel/coating interface of galvanized ultra-low-carbon

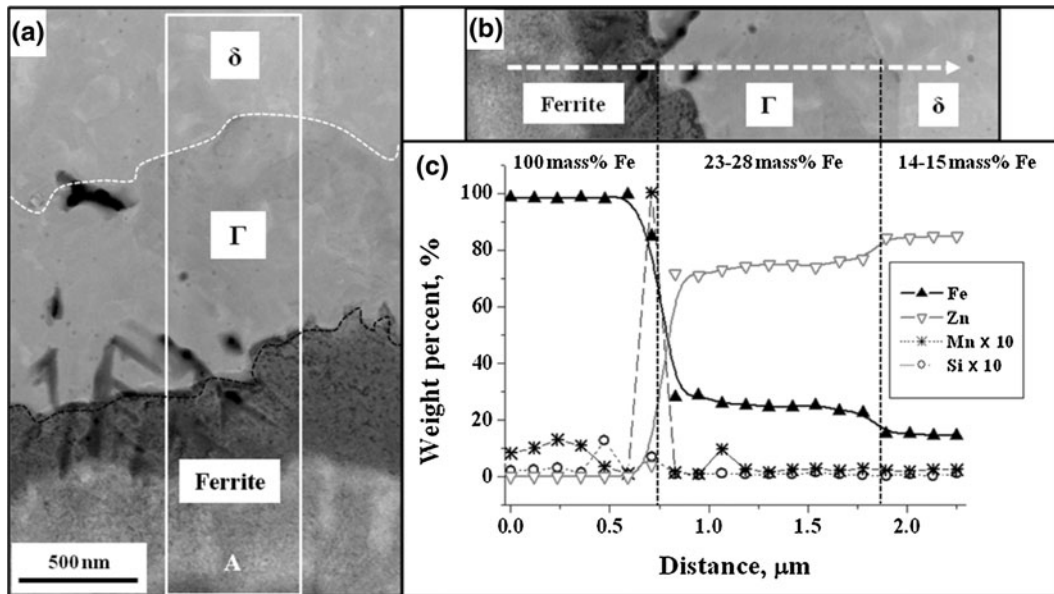


Fig. 11—Cross-sectional STEM images and EDS elemental line profiles for Fe, Zn, Mn, and Si at the steel/coating interface of the GA TRIP steel annealed in a high DP gas atmosphere of 278 K (+5 °C). (a) STEM DF image of the steel/coating interface. (b) Area labeled A in (a). (c) EDS elemental profiles for Fe, Zn, Mn, and Si at the steel/coating interface, taken along the *dashed line* in the direction of the *arrow* in (b).

Table II. Crystallographic and Compositional Data of the Studied Fe-Zn Intermetallic Phase Crystals

Phase	Structure Formula	Crystal System	Space Group	Lattice Parameters	wt pct Fe ^[2]	wt pct Fe [Present Study]
η	Zn	Hexagonal	P6 ₃ /mmc	$a = 2.6647$ nm $c = 4.9469$ nm	<0.03	
ζ	FeZn ₁₃	Monoclinic	C2/m	$a = 1.3424$ nm $b = 0.7608$ nm $c = 0.5061$ nm $\beta = 127.3$ deg	5–6	
δ_p δ_k	FeZn ₁₀ FeZn ₇	Hexagonal	P6 ₃ /mmc	$a = 1.2787$ nm $c = 5.7222$ nm	7–11.5	9–13 [coarse δ_p] 15–16 [small δ_p]
Γ_1	Fe ₁₁ Zn ₍₃₉₋₄₂₎	Face centered cubic	F $\bar{4}3$ m	$a = 1.7963$ nm	17–19.5	17–18
Γ	Fe ₃ Zn ₁₀	Body centered cubic	I $\bar{4}3$ m	$a = 0.9018$ nm	23.5–28.0	27–31

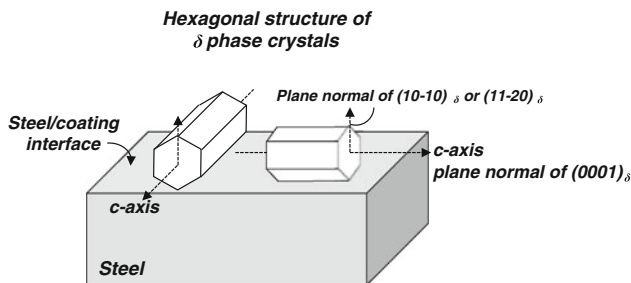


Fig. 12—Schematic drawing of the fiber texture of the δ phase crystals in a coating layer on GA steels.^[28]

steel. They reported that the Fe/Al atomic ratio of the Al-rich layer formed during the hot dipping into a Zn bath containing 0.13 mass pct Al was larger than the

value of 0.4 for Fe₂Al₅. The fine δ phase crystals formed during the galvannealing of the panels intercritically annealed in high DP gas atmospheres contained ~15 to 16 mass pct Fe (Figures 9, 10). The Fe supersaturation of the δ phase crystals is clear when the Fe content is compared to the content reported in other studies,^[2,27] as shown in Table II. Al was present at the GA coating surface and the oxides were present throughout the coating layer. The significant shift of the position of the Al and the oxides from the original steel/coating interface to the Zn-rich side during the galvannealing of the panel intercritically annealed in higher DP conditions is very likely due to the presence of a much thinner layer of the external oxides, resulting in the higher growth rate of Fe-Zn intermetallic phases. Small amounts of coarse δ phase crystals were also observed in

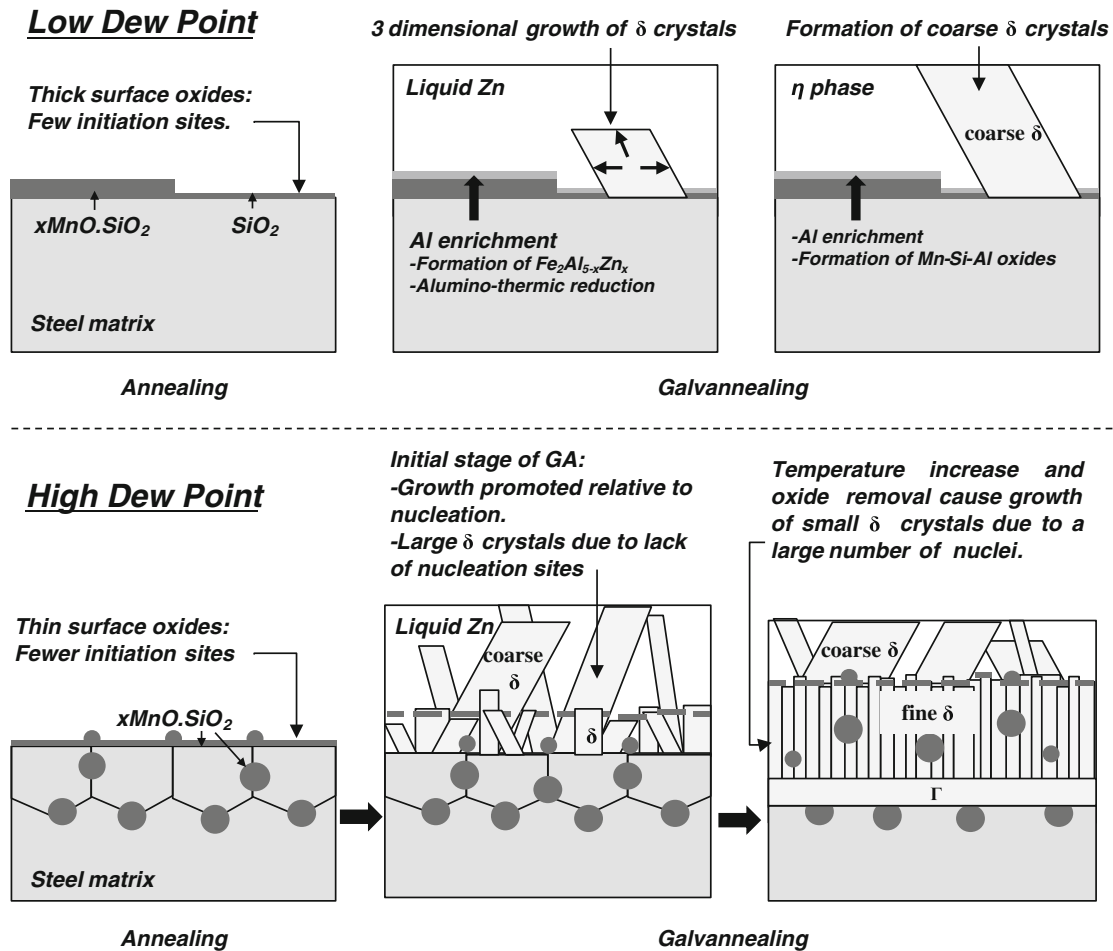


Fig. 13—Schematic drawing of the mechanism for the formation of Fe-Zn intermetallic phase crystals during galvannealing of a CMnSi TRIP steel annealed in low DP and high DP conditions.

the upper part of the coating layer of the panel intercritically annealed in high DP [273 K and 278 K (0 °C and +5 °C)] gas atmospheres (Figures 9, 10). These δ phase crystals were very likely formed in the initial stage of the galvannealing, when the growth rate of Fe-Zn intermetallic phases was slow due to the lower galvannealing temperature and the presence of a thin layer of external oxides at the steel/coating interfaces. This explains why the coarse δ phase crystals had a lower Fe content than the fine δ phase crystals and that no oxides were present in the coarse phase crystal.

The Al contained in the Zn bath reacted with the Mn-Si surface oxides to form Mn-Si-Al ternary compound oxides and did not remain in solid solution in the Zn (Figure 6). The Mn-Si-Al oxides were also observed close to the coating surface (Figure 9). This shows that the Al migrated to the coating surface not by diffusion of elemental Al, but as part of a Mn-Si-Al oxide during the galvannealing reaction. It has been known for some time that MnO formed at the steel surface can be reduced by the Al contained in the Zn bath during hot dipping and that this reaction removes some of the surface oxides, resulting in the improved wettability of the strip by the molten Zn.^[34,35] Thermodynamic data clearly show that the Al_2O_3 is more stable than SiO_2

and MnO at 733 K (460 °C).^[36,37] Thus, SiO_2 and $xMnO \cdot SiO_2$ oxides can also be reduced by Al. The observation of the Mn-Si-Al oxides supports the view that the solute Al in the Zn also reacted with the surface oxides during the galvannealing process. These observations represent a strong agreement in favor of alumino-thermic reduction of the Mn-Si compound oxides in continuous galvanizing. The Mn-Si-Al oxides observed in the present study are likely the intermediate product of the alumino-thermic reduction.

The morphology and size of the δ phase crystals were also clearly influenced by the DP gas atmosphere. At the coating surface of the panel intercritically annealed in the 213 K (−60 °C) DP gas atmosphere, coarse δ phase crystals were observed. They were single crystals with a random orientation and did not have a preferential growth direction. At the surface of the panel intercritically annealed in the 278 K (+5 °C) DP atmosphere, the coating consisted mainly of a compact layer of fine δ phase crystals. They grew vertically, *i.e.*, normal to the original steel/coating interface. The panel intercritically annealed at 263 K (−10 °C) DP gas atmosphere had coarse δ phase crystals in the upper part of the coating layer and fine δ phase crystals were observed in the lower part of the coating layer.

The schematics of Figure 13 illustrate the mechanism of the formation of δ phase crystals in the presence of Mn-Si compound oxides during galvannealing of the TRIP steel annealed in low and high DP conditions. The reason for the observation of a difference in the morphology of the δ phase crystals after IA in gas atmosphere with different DPs is related to the initiation of the Fe-Zn reaction at the steel/Zn interface. After IA in a low DP gas atmosphere, a thick layer of the Mn-Si compound oxides covers the surface fully. As a result, the free surface area where Fe and Zn can directly interact with each other and react to form the intermetallic phases is very small, and the number of the initiation sites for the Fe-Zn reaction leading to the formation of δ phase crystals is small. In this situation, the growth of the very few δ phase crystals which are nucleated is not hindered by the growth of other δ phase crystals. Consequently, large δ phase crystals are formed.

IA in a high DP atmosphere results in a thin layer of external oxidation. More initiation sites for the Fe-Zn reaction are available at the surface. In the initial stage of the galvannealing, the number of reaction initiation site is smaller due to the presence of the Mn-Si surface oxides. Relatively coarse δ phase crystals are, therefore, formed initially. The oxides are rapidly removed by the Fe-Zn reaction and many δ phase crystals with random orientations are formed simultaneously at the steel/coating interface. The δ phase crystals aligned with their fastest growth direction normal to the original steel/coating interface will have a high growth rate and will experience limited interference from other δ phase crystals in the growth direction. This results in the preferential growth of δ crystals with a fast growth direction in the direction normal to the original steel/coating interface. In the lower part of the coating layer, fine δ phase crystals with a columnar morphology are present, whereas the upper part of the coating layer consists of coarse δ phase crystals. A crystallographic fiber texture by geometrical selection is often observed when growth in a specific crystallographic direction is much faster than the other directions.^[38] In the case of the δ phase crystals, this direction is $\langle 10\bar{1}0 \rangle_{\delta}$ or $\langle 11\bar{2}0 \rangle_{\delta}$.

A high DP IA gas atmosphere is therefore effective in causing the faster interdiffusion of Fe and Zn during the galvannealing of a CMnSi TRIP steel. The galvannealing coating quality is significantly influenced by the thickness of the external oxide layer. The formation of internal oxides formed during IA in a high DP atmosphere does not significantly disturb the diffusion of Fe and Zn and the formation of the δ phase during galvannealing.

V. CONCLUSIONS

The Fe-Zn reaction occurring during the galvannealing of a CMnSi TRIP steel was investigated. After the hot dip galvannealing of a panel intercritically annealed in low DP gas atmospheres, the coating layer consisted of η and δ phase crystals. After the galvannealing of a panel annealed in higher DP gas atmospheres, the

coating layer consisted δ and Γ phase crystals, and a thin layer of Γ phase crystals was present at the steel/coating interface. The selective oxides were distributed homogeneously throughout the GA coating layer. The reduction of the thickness of the surface oxides' layer on panels intercritically annealed in a high DP gas atmosphere resulted in a higher Fe content at the surface of the GA layer. The improved coating quality of the panels intercritically annealed in higher DP gas atmospheres is due to internal oxidation. IA in high DP atmospheres accelerates the Fe-Zn reaction kinetics during the galvannealing of CMnSi TRIP steel processed in hot dip galvannealing lines. This reduces the number of Zn-alloy coating defects and improves the control of the Zn coating properties related to coating adhesion and powdering resistance.

ACKNOWLEDGMENTS

The authors gratefully acknowledge the support of the POSCO Technical Laboratories, Gwangyang, South Korea.

REFERENCES

1. C.E. Jordan, K.M. Goggins, and A.R. Marder: *Metall. Mater. Trans. A*, 1994, vol. 25A, pp. 2101–09.
2. A.R. Marder: *Prog. Mater. Sci.*, 2000, vol. 45, pp. 191–271.
3. B. Mintz: *Int. Mater. Rev.*, 2001, vol. 46, pp. 169–97.
4. L. Chen, H.S. Kim, S.K. Kim, and B.C. De Cooman: *ISIJ Int.*, 2007, vol. 47, pp. 1804–12.
5. I. Hertveldt, B.C. De Cooman, and S. Claessens: *Metall. Mater. Trans. A*, 2000, vol. 31A, pp. 1225–32.
6. S. Feliu and M. Pérez-Revenga: *Acta Mater.*, 2005, vol. 53, pp. 2857–66.
7. M. Blumenau, M. Norden, F. Friedel, and K. Peters: *Steel Res. Int.*, 2010, vol. 81, pp. 1125–36.
8. Y.F. Gong, H.S. Kim, and B.C. De Cooman: *ISIJ Int.*, 2008, vol. 48, pp. 1745–51.
9. Y.F. Gong, H.S. Kim, and B.C. De Cooman: *ISIJ Int.*, 2009, vol. 49, pp. 557–63.
10. L. Cho, M.S. Kim, Y.H. Kim, S.J. Lee, and B.C. De Cooman: *Proc. 8th Int. Conf. Zinc Zinc Alloy Coated Steel Sheet (GALVATECH 2011)*, Genova, Italy, Associazione Italiana di Metallurgia, Milano, 2011, pp. 145–52.
11. J. Mahieu, S. Claessens, and B.C. De Cooman: *Metall. Mater. Trans. A*, 2001, vol. 32A, pp. 2905–2908.
12. X.V. Eynde, J.P. Servais, and M. Lamberigts: *Surf. Interface Anal.*, 2003, vol. 35, pp. 1004–14.
13. J. Mahieu, S. Claessens, B.C. De Cooman, and F. Goodwin: *6th Int. Conf. Zinc Zinc Alloy Coated Steel Sheet (GALVATECH 2004)*, Chicago, Illinois, 2004. Association for Iron and Steel Technology, Warrendale, 2004, pp. 529–38.
14. X.S. Li, S.I. Baek, C.S. Oh, S.J. Kim, and Y.W. Kim: *Scripta Mater.*, 2007, vol. 57, pp. 113–16.
15. L. Cho, S. Lee, M. Kim, Y. Kim, and B.C. De Cooman: *Metall. Mater. Trans. A*, 2013, vol. 44A, pp. 362–71.
16. D. Huin, P. Flauder, and J.B. Leblond: *Oxid. Met.*, 2005, vol. 64, pp. 131–67.
17. J. Nakano, D.V. Malakhov, S. Yamaguchi, and G.R. Purdy: *CALPHAD*, 2007, vol. 31, pp. 125–40.
18. J. McDerimid, M. Kaye, and W. Thompson: *Metall. Mater. Trans. B*, 2007, vol. 38B, pp. 215–30.
19. P. Shewmon, M. Abbas, and G. Meyrick: *Metall. Trans. A*, 1986, vol. 17A, pp. 1523–27.
20. J. Dohie, J.R. Cahoon, and W.F. Caley: *J. Phys. Equal Differ.*, 2007, vol. 28, pp. 322–27.

21. H. Liu, Y. He, S. Swaminathan, M. Rohwerder, and L. Li: *Surf. Coat. Technol.*, 2011, vol. 206, pp. 1237–43.
22. R.W. Lynch and H.G. Drickamer: *J. Phys. Chem. Solids*, 1965, vol. 26, pp. 63–68.
23. R. Belin, M. Tillard, and L. Monconduit: *Acta Crystallogr. C*, 2000, vol. 56, pp. 267–68.
24. C. Belin and R. Belin: *J. Solid State Chem.*, 2000, vol. 151, pp. 85–95.
25. A. Koster and J. Schoone: *Acta Crystallogr. B*, 1981, vol. 37, pp. 1905–1907.
26. J. Brandon, R. Brizard, P. Chieh, R. McMillan, and W. Pearson: *Acta Crystallogr. B*, 1974, vol. 30, pp. 1412–17.
27. J. Mackowiak and N. Short: *Int. Met. Rev.*, 1979, vol. 24, pp. 1–19.
28. V. Rangarajan, C.C. Cheng, and L.L. Franks: *Surf. Coat. Technol.*, 1993, vol. 56, pp. 209–14.
29. G.F. Bastin, F.J.J. van Loo, and G.D. Rieck: *Zeitschrift fuer Metallkunde/Mater. Res. Adv. Tech.*, 1976, vol. 67, pp. 694–98.
30. V. Raghavan: *J. Phys Equilibria Diffus.*, 2013, vol. 34, pp. 1–3.
31. M. Onishi, Y. Wakamatsu, and H. Miura: *Trans. Jpn Inst. Met.*, 1974, vol. 15, pp. 331–37.
32. P. Munroe, C. Laksmi, and B. Gleeson: *Mater. Sci. Eng. A*, 1998, vol. 251, pp. 87–93.
33. E. Baril and G. L'espérance: *Metall. Mater. Trans. A*, 1999, vol. 30A, pp. 681–95.
34. R. Khondker, A. Mertens, and J.R. McDermid: *Mater. Sci. Eng. A*, 2007, vol. 463, pp. 157–165.
35. R. Kavitha and J.R. McDermid: *Proc. 8th Int. Conf. Zinc Zinc Alloy Coated Steel Sheet (GALVATECH 2011), Genova, Italy*. Associazione Italiana di Metallurgia, Milano, 2011, vol., pp. 1243–53.
36. F. Li, H. Liu, W. Shi, and L. Li: *J. Coat. Technol. Res.*, 2011, vol. 8, pp. 639–47.
37. Y.F. Gong, T.J. Song, H.S. Kim, J.H. Kwak, and B.C. De Cooman: *Proc Asia Pacific Galvanizing Conf., Jeju, Korea*. The Corrosion Science Society of Korea, paper no. B-15, 2009.
38. V. Radmilovic, U. Dahmen, D. Gao, C.R. Stoldt, C. Carraro, and R. Maboudian: *Diam. Relat. Mater.*, 2007, vol. 16, pp. 74–80.